Supplementary Information

Pressure-stabilized GdN_6 with armchair-antiarmchair structure as a high energy density material

Lulu Liu[1,3], Dinghui Wang[1,3], Shoutao Zhang[*,2], and Haijun Zhang[†,1,3]

[1]*National Laboratory of Solid State Microstructures, School of Physics, Nanjing University, Nanjing 210093, China*

[2]*Centre for Advanced Optoelectronic Functional Materials Research and Key Laboratory for UV Light-Emitting Materials and Technology of Ministry of Education, Northeast Normal University, Changchun 130024, China*

[3]*Collaborative Innovation Center of Advanced Microstructures, Nanjing University, Nanjing 210093, China*

Address correspondence to: [*]zhangst966@nenu.edu.cn; [†]zhanghj@nju.edu.cn

Index **Page**

Computational Details

We employed the unbiased swarm intelligence structure prediction method as implemented in CALYPSO code.[1,2] Herein, we have performed structural searches Gd-N compounds with various Gd_xN_y (x = 1, y = 1-6; and x = 2, y = 2, 3) compositions with simulation cell size up to 4 formula units (f.u.) at 0 K and selected pressures of 1 atm, 25, 50, and 100 GPa. In the first step, random structures with certain symmetry are constructed in which atomic coordinates are generated by the crystallographic symmetry operations. Local optimizations using the VASP code[3] were done with the conjugate gradients method and stopped when enthalpy changes became smaller than 1×10^{-5} eV per cell. After processing the first generation structures, 60% of them with lower enthalpies are selected to construct the next generation structures by PSO (Particle Swarm Optimization). 40% of the structures in the new generation are randomly generated. A structure fingerprinting technique of bond characterization matrix is applied to the generated structures, so that identical structures are strictly forbidden. These procedures significantly enhance the diversity of the structures, which is crucial for structural global search efficiency.

To further analyze the structures with higher accuracy, we select a number of structures with lower enthalpies and perform structural optimization using density functional theory within the generalized gradient approximation[4] as implemented in the VASP code. The cut-off energy for the expansion of wavefunctions into plane waves is set to 600 eV in all calculations, and the Monkhorst-Pack k-mesh with a maximum spacing of 0.025 $Å^{-1}$ was individually adjusted in reciprocal space with respect to the size of each computational cell. This usually gives total energy well converged within ~1 meV/atom. The electron-ion interaction was described by means of projector augmented wave with $4f^{7}5d^{1}6s^{2}$ and $2s^{2}2p^{3}$ valence electrons for Gd and N atoms, respectively. To prove that the GdN_6 is ferromagnetic under1 atm. We constructed different magnetic configurations and calculated the enthalpy. The Coulomb U parameters with 4.5 eV were applied to the Gd f orbits, the

quasi-harmonic model[5] was adopted to calculate the phonon spectra using the supercell method.

Supplementary Figures

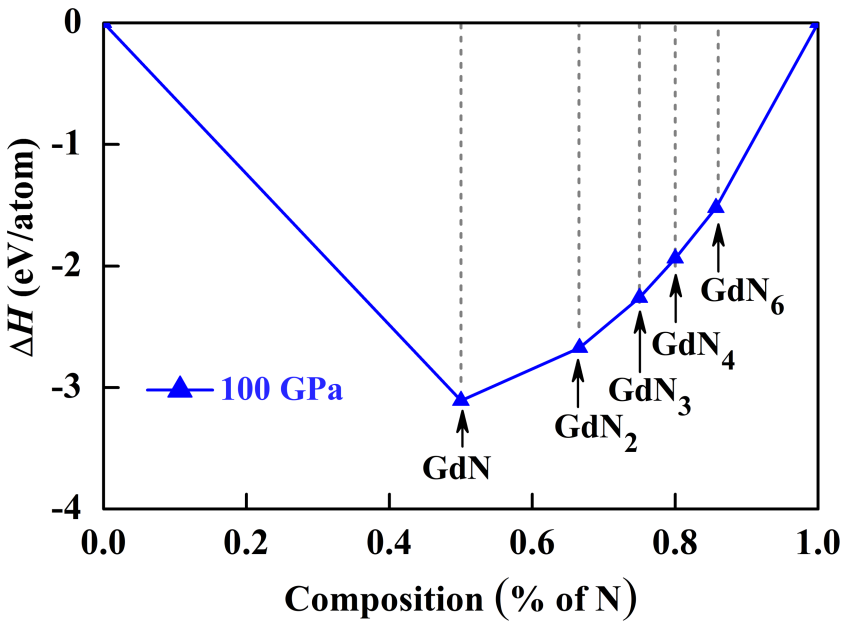

Fig. S1. Convex hulls for formation enthalpies (ΔH, with respect to pure Gd and N_2) at 100 GPa, calculated with the PBE +DFT-D3 functional.

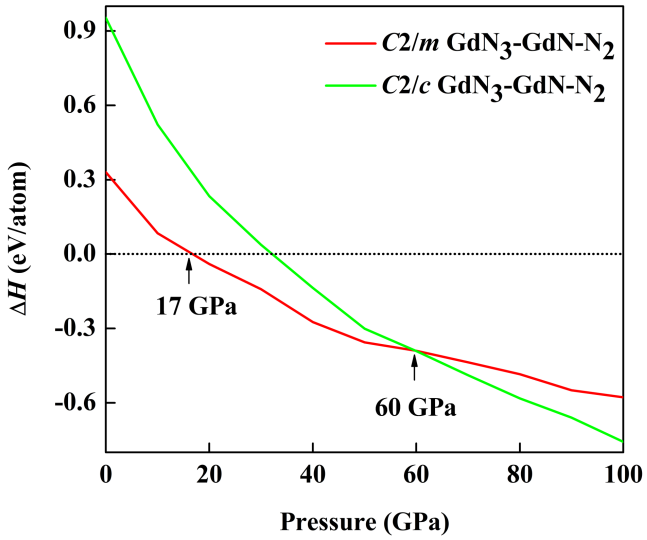

FIG. S2. The enthalpy differences of *C*2/*m* phase and *C*2/*c* phase GdN_3 relative to *Fm*-3*m* GdN and nitrogen.

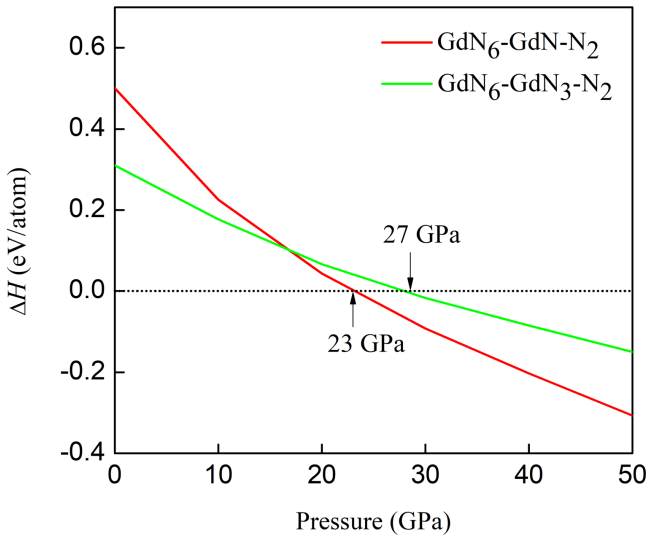

Fig. S3. The enthalpy differences of *P*-1 GdN_6 relative to *Fm*-3*m* GdN or *C*2/*m* GdN_3 and nitrogen phases.

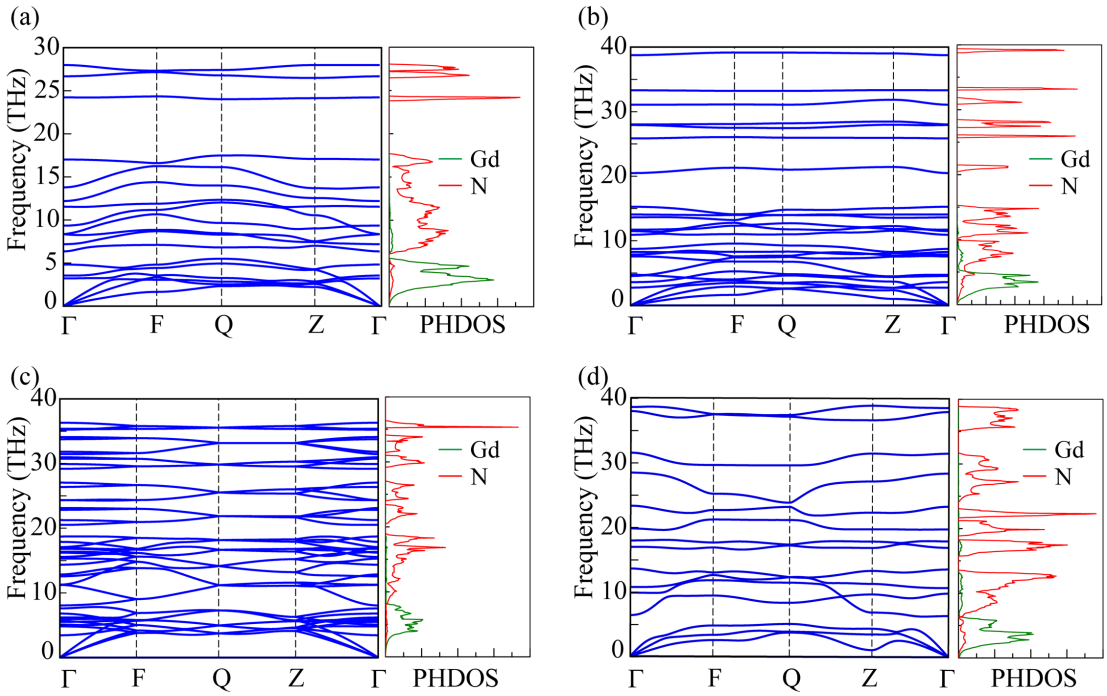

Fig. S4. Phonon dispersion and phonon density of states (PHDOS) projected on Gd and N atoms. (a) Phonon dispersion and PHDOS of *P*-1 GdN_2 at 1 atm. (b) Phonon dispersion and PHDOS of *C*2/*m* GdN_3 at 1 atm. (c) Phonon dispersion and PHDOS of *C*2/*c* GdN_3 at 100 GPa. (d) Phonon dispersion and PHDOS of *P*-1 GdN_4 at 50 GPa.

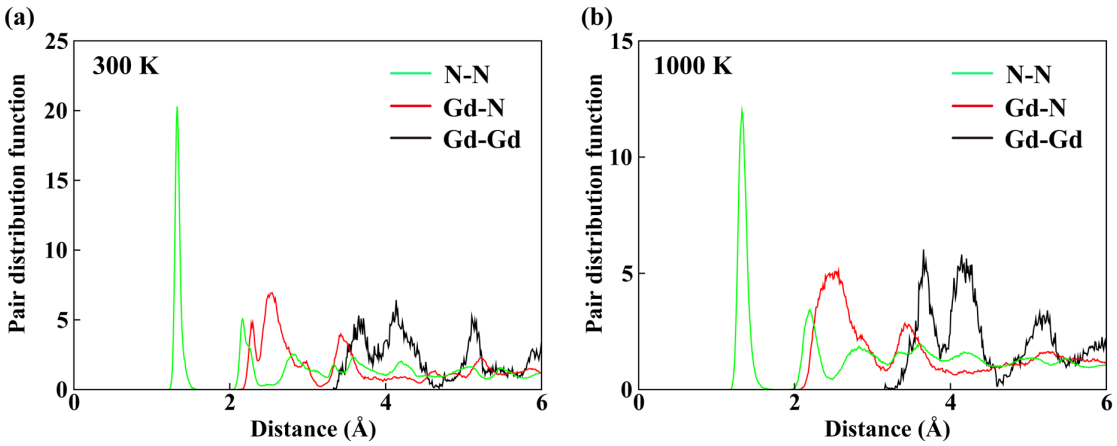

Fig. S5. Pair distribution functions of AIMD simulations at 27 GPa and temperatures of 300 (a) and 1000 K (b), where the green, red, and black lines represent the N-N, Gd-N, and Gd-Gd pairs, respectively.

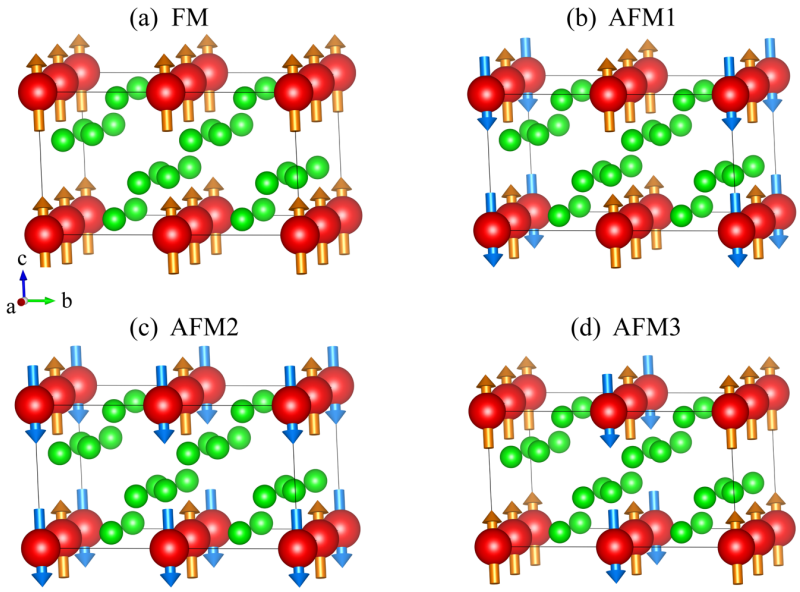

Fig. S6. Different magnetic configurations of *P*-1 GdN_6 at 1atm. The yellow arrow and blue arrow indicate that the magnetic are along the (001) and (0 0 -1) direction, respectively. (a) Ferromagnetic (FM) structures and (b)-(d) antiferromagnetic (AFM) structures, whereas, we named the different antiferromagnetic configurations in order of AFM1, AFM2, and AFM3, respectively.

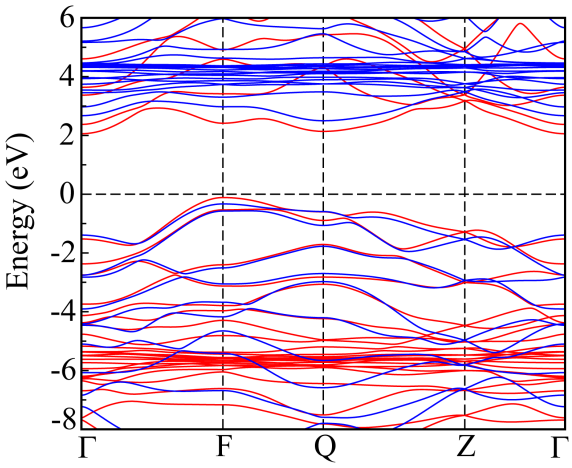

Fig. S7. Electronic band structure of *C*2/*c* GdN_3 at 100 GPa, where, the horizontal dashed line represents the Fermi level. The spin-up and spin-down electron energy bands are represented by red and blue lines, respectively.

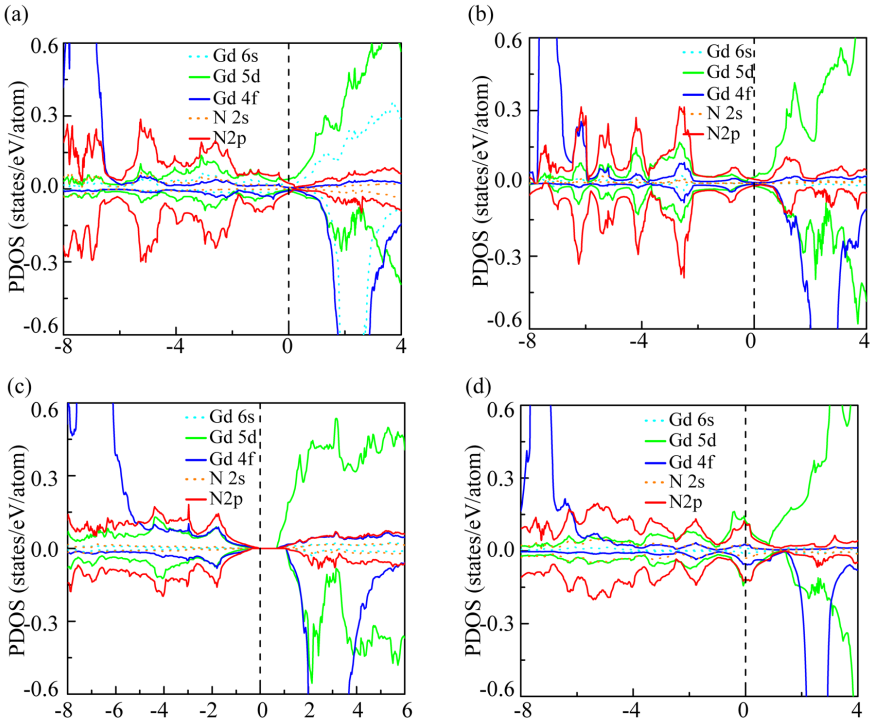

Fig. S8. Projected density of states (PDOS) of stable Gd-N compound under different pressures, where the horizontal dashed line represents the Fermi level. (a) PDOS of *P*-1 GdN_2 at 1 atm. (b) PDOS of *C*2/*m* GdN_3 at 1 atm. (c) PDOS of *C*2/*c* GdN_3 at 100 GPa. (d) PDOS of *P*-1 GdN_4 structures at 50 GPa.

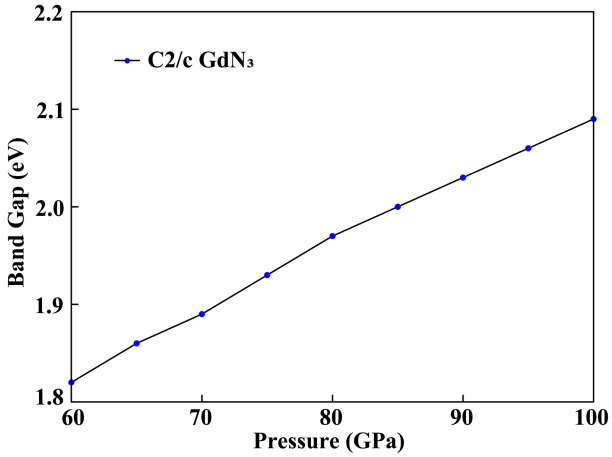

Fig. S9. Pressure dependence of electronic bandgaps of *C*2/*c* GdN_3.

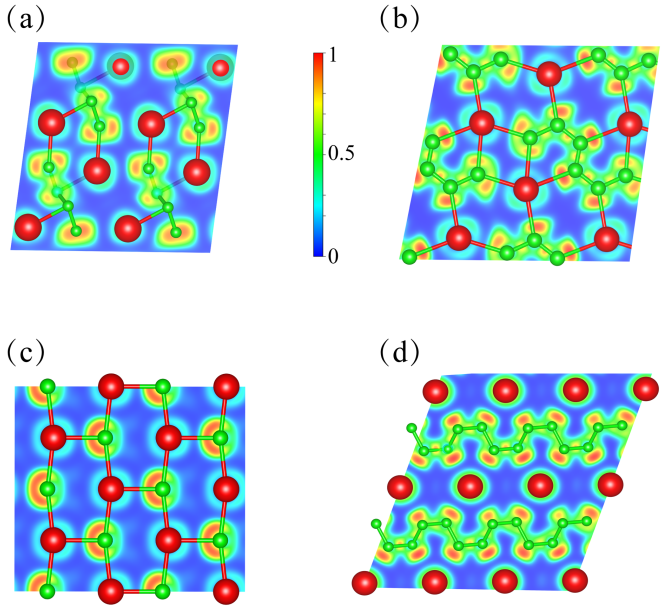

Fig. S10. (a) ELF of *P*-1 GdN_2 at 1 atm. (b) ELF of *C*2/*m* GdN_3 at 1 atm. (c) ELF of *C*2/*c* GdN_3 at 100 GPa. (d) ELF of *P*-1 GdN_4 at 50 GPa.

Supplementary Tables

Table S1. Structural parameters of predicted stable Gd-N compounds.

Phases	Pressure	Lattice Parameters (Å)	Atoms	Wyckoff Positions (fractional)		
				x	*y*	*z*
$P\bar{1}$ -GdN_6	1 atm	*a* = 4.4492	Gd(1a)	0.0000	0.0000	0.0000
		b = 4.0110	N1(2i)	0.7115	0.7161	0.3356
		c = 4.51260	N2(2i)	0.4660	0.9029	0.3678
		α = 95.3508	N3(2i)	0.3480	0.5027	0.9179
		β = 102.7453				
		γ = 89.3554				
$P\bar{1}$ -GdN_4	50 GPa	*a* = 3.6030	Gd(2i)	0.0000	0.0000	0.5000
		b = 3.8972	N1(2i)	0.4635	0.5258	0.1562
		c = 4.07880	N2(2i)	0.6281	0.14876	88403
		α= 76.0914				
		β = 100.9941				
		γ = 107.2000				
*C*2/*m* -GdN_3	1 atm	*a* = 3.6702	Gd(2i)	0.7200	0.2916	0.6937
		b = 3.6985	N1(2i)	0.8366	0.1571	0.3484
		c = 6.9712	N2(2i)	0.7281	0.2718	0.1801
		α= 99.1387	N3(2i)	0.8843	0.1203	0.0009
		β = 82.2202				
		γ = 96.6750				
*C*2/*c* -GdN_3	100 GPa	*a* = 4.7007	Gd(4e)	0.1631	0.2916	1.2500
		b = 5.2873	N1(8f)	0.1229	0.4496	0.9586
		c = 4.9874	N2(4e)	0.0000	0.7145	1.2500
		α=*γ* = 90.000				
		β = 100.2624				
$P\bar{1}$ -GdN_2	1 atm	*a* = 3.5043	Gd(2i)	0.6910	0.7594	0.7717
		b = 3.8124	N1(2i)	0.8175	0.7279	0.1986
		c = 5.6592	N2(2i)	0.9391	0.3297	0.5563
		α= 85.6921				
		β = 103.1098				
		γ = 91.3368				

Table S2. The enthalpy differences between FM and AFM for *P*-1 GdN_6 at 1atm.

	H_{FM}-H_{AFM1}	H_{FM}-H_{AFM2}	H_{FM}-H_{AFM3}
Δ*H* (meV/f.u.)	-0.46	-0.28	-0.29

Table S3. The ICOHP values for the shortest Gd-N and N-N bonds of the *P*-1 GdN_4 at 50 GPa, *C*2/*m* GdN_3 at 1 atm, *C*2/*c* GdN_3 at 100 GPa, and *P*-1 GdN_2 at 1atm.

	$P\bar{1}$ -GdN_4	*C*2/*m* -GdN_3	*C*2/*c* -GdN_3	$P\bar{1}$-GdN_2
Gd-N (eV/pair)	-0.41	-0.38	-0.18	-0.32
N-N (eV/pair)	-1.04	-0.7	-1.0	-1.06

Table S4. Detonation properties of the predicted *P*-1 GdN_4, *C*2/*m* GdN_3, *C*2/*c* GdN_3, and *P*-1 GdN_2. ρ, E_d, E_v, V_d, and P_d mean density, chemical energy density, the volumetric energy densities, detonation velocity, and detonation pressure, respectively.

	ρ (g/cm^3)	E_d (kJ/g)	E_v (kJ/cm^3)	V_d (km/s)	P_d (kbar)
$P\bar{1}$ -GdN_4	6.71	0.32	2.15	8.01	468
*C*2/*m* -GdN_3	7.2	0.69	4.97	8.73	561
$P\bar{1}$ -GdN_2	8.4	0.56	4.70	7.01	373

References

(1) Wang, Y.; Lv, J.; Zhu, L.; Ma, Y. CALYPSO : A Method for Crystal Structure Prediction. *Comput. Phys. Commun.* **2012**, *183*, 2063.

(2) Wang, Y.; Lv, J.; Zhu, L.; Ma, Y. Crystal Structure Prediction via Particle-Swarm Optimization. *Phys. Rev. B* **2010**, *82*, 094116.

(3) Kresse, G.; Furthmiiller, J. Efficiency of Ab-Initio Total Energy Calculations for Metals and Semiconductors Using a Plane-Wave Basis Set. *Comput. Mater. Sci.* **1996**, *6*, 15–50.

(4) Perdew, J.; Chevary, J.; Vosko, S.; Jackson, K.; Pederson, M.; Singh, D.; Fiolhais, C. Atoms, Molecules, Solids, and Surfaces: Applications of the Generalized Gradient Approximation for Exchange and Correlation. *Phys. Rev. B* **1992**, *46*, 6671.

(5) Togo, A.; Oba, F.; Tanaka, I. First-Principles Calculations of the Ferroelastic Transition between Rutile-Type and CaCl2-Type SiO2 at High Pressures. *Phys. Rev.* B 2008, 78, 134106.